LETTER • OPEN ACCESS

Augmenting the spatial resolution of climate-change temperature projections for city planners and local decision makers

To cite this article: Juan Diego Jijón *et al* 2021 *Environ. Res. Lett.* **16** 054028

View the article online for updates and enhancements.

ENVIRONMENTAL RESEARCH
LETTERS

Augmenting the spatial resolution of climate-change temperature projections for city planners and local decision makers

Juan Diego Jijón[1,*] ![ORCID], Karl-Heinz Gaudry[1,2] ![ORCID], Jessica Constante[1] ![ORCID] and César Valencia[3]

1   Instituto de Investigación Geológico y Energético (IIGE), Quito, Ecuador
2   Center for International Migration (GIZ/CIM), Eschborn, Germany
3   Programa de Ciudades Intermedias Sostenibles, Deutsche Gesellschaft für Internationale Zusammenarbeit (GIZ) GmbH, Quito, Ecuador
*   Author to whom any correspondence should be addressed.

E-mail: juan.jijon@geoenergia.gob.ec **and** karl.gaudry@geoenergia.gob.ec

Keywords: satellite imagery, climate change, downscaling methods, urban, land-use planning

Abstract

Before the 2010, studies in climate change (CC) projections embracing scales below $3°$ were difficult to find. This has changed dramatically over the past ten years, with literature addressing high resolution grids for climate studies, allowing a better understanding and forecasting of CC at finer scales. However, downscaling methods remain poorly explored in urban planning. Research shows that the main difficulties relate to mismatches between data needs and data availability, terminology, constraints of information technology and maps that inform spatial planning decision-making processes. Based on dynamic downscaled maps for RCP 4.5 and RCP 8.5 at 10 km resolution published by Ecuador's Ministry of Environment and Water (MAAE), we develop a method for augmenting the resolution scale at 30 m. We use digital elevation models and Landsat 4/5/7/8 satellite imagery for land surface temperature (LST) and present a series of steps and equations before applying Stefan Bolzman's law. We present the necessary equations between the filling-in of LST outliers, and their projection onto air temperature at 2 m height, taking surface emissivity estimates based on (Alves *et al* 2017 *J. Hyperspectral Remote Sens.* **7** 91–100). We extrapolate the resulting air temperature in time with Fourier's series, and for the purpose of coherence among scales, we upscale air temperature maps at 30 m to those at 10 km resolution. The resulting CC projection maps are validated with the temporal series of air temperature (max, min, mean) from the meteorological station in the Ecuadorian city of Portoviejo (Student's t-test) for the period between 1981 and 2005, with Portoviejo city facing temperature increases of up to 2 °C under RCP 4.5 scenario in the period 2011–2040 vs 1981–2005. The final CC maps have an augmented resolution of 30 m, are compatible with those of MAAE, and offer a low-cost procedure for informing land-use and urban planners, as well as local development decision makers, of temperature anomalies due to climate change.

1. Introduction

With the forecast of 6.3 billion persons living in urban areas by 2050, it is expected that problems associated with the use of natural resources and the negative externalities of anthropogenic activity will become increasingly relevant. From the point of view of climate studies, this context highlights the need for downscaling methods and procedures in order to accurately assess and depict scenarios for climate change (CC) at urban/local scales of 12.5–50 km and

below [1]. However, downscaling methods remain poorly explored in urban planning because urban planners and climatologists do not usually work together to tackle the effects of CC at small scales. The main difficulties relate to mismatches between data needs and data availability, terminology (which is not unified), constraints of information technology [1] and maps that inform spatial planning decision-making processes.

The advancement of computational resources and the combination of diversified strategies of dynamical

and statistical downscaling (DDS and SDS) have boosted the field of CC studies, particularly since the beginning of the 2010s. At the same time, the development of the Global Climate Models, under the scope of the IPPC standards, combined with the creation of regional models, applied to several objectives (such as assessing the effects of temperature and precipitation variability on land use) has encouraged the emergence of specific models applied to increasingly higher resolution scales.

In Latin America, and especially Ecuador, several institutional frameworks have been developed which seek to incorporate CC criteria into public management at various sectors and scales.

In the case of Ecuador, the National Climate Change Strategy recognizes the importance of including the different sectors and administrative units, from the central government down to the municipalities or 'Decentralized Autonomous Governments' (GADs). As a result of the UN-Habitat III Conference in 2016, the bilateral cooperation agreement between the governments of Germany and Ecuador, and within the frameworks of its program 'Intermediate Sustainable Cities' (CIS), the Ministry of Urban Development and Housing in Ecuador and its counterpart, the German Technical Cooperation (GIZ), have collaborated with other ministries such as the Ministry of Environment and Water (MAAE). Their aim is to improve the enabling conditions for sustainable urban development, within the framework of the New Urban Agenda (NUA), the Sustainable Development Goals and the Paris Agreement. Initiatives for incorporating CC into the local development narrative have so far been addressed mostly in CIS's city-partners (Ambato, Cuenca, Lago Agrio, Latacunga, Loja and Portoviejo). However, land-use planning at several administrative scales, particularly when considering the Paris Agreement and the NUA, still require low-cost methods and procedures that accurately assess and depict scenarios for CC at urban/local scales. Additionally, if CC projections are to be incorporated into the spatial planning processes and be used by the spatial planning departments at municipal level, municipal departments and technicians require spatial representations of CC and of the relationships between the land-use planning elements.

Before 2010, studies embracing scales below 3° of latitude were difficult to find. This has dramatically changed over the past ten years, with literature addressing high resolution grids for climate studies, allowing a better understanding and forecasting of CC at finer scales. Nevertheless, further advances in this field are constrained by procedures related to big data, data mining, stochastic processes, and the problem of reliability. Despite these challenges, the models developed so far have paved the way for new combinations of approaches and techniques associated with specific problems of urban and rural settlements. In

the urban areas, especially, where more than 60% of the global population lives, CC will pose increasing and escalating challenges that will affect safety, health and mobility aspects of the human routine. For this reason, CC studies at local scales are becoming pivotal, with a focus on land-use and land-change planning. In this context, SDS and DDS (SDS and DDS) methods, based on robust sets of data, and the evolution of analytical resources with satellite imagery, may help planners and managers to better deal with CC at small scales.

For the purpose of narrowing our focus to the CC and land-use planning nexus, we first carried out a review of the literature examining which downscaling methods/models/tools are available, and how these have been used for spatial and land-use planning purposes. Our search strategy involved academic data bases (Science Direct, Emerald, Google Scholar and Taylor & Francis) and included the expressions 'downscale method' AND 'climate change' AND 'land use' AND 'planning'. Our selection of articles excluded those that were duplicated or incomplete, research posters, studies larger than six degrees of latitude, and those which had not undergone a peer review process. Based on these results (N:468 papers) we screened and reviewed 33 articles that addressed scales (a) from 99 km to 5 km; and (b) below 5 km (see table 1).

In addition to the literature review, we considered the advances made in Ecuador, in terms of its climate projections under the different emission scenarios. As part of its Third National Communication on Climate Change to the United Nations Framework Convention on Climate Change, MAAE produced a series of maps reflecting the climate projections for Ecuador under emission scenarios 2.6, 4.5, 6.0 and 8.5.

As part of its downscaling methods, MAAE considered approximately 15 global climate models, and selected finally four models (IPSL-CM5A-MR, MIROC-ESM, GISS-E2-R and CSIRO-Mk3-6-0), that best describe the atmospheric dynamics of the country. MAAE developed and published two types of scale reduction: (a) statistical (assembling the models of IPSL-CM5A-MR, MIROC-ESM, GISS-E2-R and CSIRO-Mk3-6-0); and (b) dynamic. Its statistical scale reductions were obtained for precipitation parameters, maximum, average and minimum temperatures for the Representative Concentration Pathway (RCP) 2.6, 4.5, 6.0, 8.5 scenarios in the historical (1981–2005) and future (2011–2100) periods. In addition to the selection of global climate models, dynamic scale reductions used the regional model called Weather Research and Forecasting (WRF) version 3.61 [35]. As a result, MAAE generated a series of climate projection maps at a resolution of 10 km (10×10 km) on a daily and monthly scale, for the parameters: (a) precipitation, (2) temperature, (3) relative humidity, (4) wind, and (5) radiation for the

Table 1. Climate change downscaling studies and scales (a) between 99 km and 5 km and (b) below 5 km.

Climate change downscaling studies and scales	
(a) Scales from 99 km to 5 km	(b) Scales below 5 km
Adham *et al* (20 km) [2], Aich *et al* (50 km) [3], Akhter *et al* (10 km) [4], Didovets *et al* (50 km) [5], Fitzpatrick and Dunn (50 km) [6], Gu *et al* (50 km) [7], Jahangir and Moghin (50 m) [8], Khalyani *et al* (40 km) [9], Kjellström *et al* (48.8 km) [10], Mathis *et al* (12 km) [11], McCarthy *et al* (25 km) [12], Oliveira *et al* (20 km) [13], Prömmel *et al* (50 km) [14], Ramyar *et al* (50 km–10 m) [15], Rodríguez-Lloveras *et al* (10 km) [16], Sanjay *et al* (50 km) [17], Seiler *et al* (83.4 km) [18], Shastri *et al* (36 km, 12 km, 4 km) [19], Su *et al* (50 km) [20], Su *et al* (48.8 km) [21], Tang *et al* (60 km–20 km) [22], Varikoden *et al* (50 km) [23], Wang *et al* (10 km) [24], Zhou (25 km) [25]	Argüeso *et al* (2 km) [26], Bastin *et al* (1.8 km) [27], Hasan *et al* (2 m) [28], Hamdi *et al* (4 km–1 km) [29], Kusaka *et al* (3 km) [30], Lauwaet *et al* (2 m) [31], Lemonsu *et al* (2 m) [32], Reshmidevi *et al* (30 m) [33], Yan *et al* (90 m) [34]
Total: 24	Total: 9

Table 2. Portoviejo watershed extension studied in this work.

Point	Longitude	Latitude
1	−80.93003	−0.769946
2	−79.85987	−0.769946
3	−80.93003	−1.360139
4	−79.85987	−1.360139

RCP 4.5 and 8.5 scenarios in the historical period (1981–2005) and the future (2011–2070).

While MAAE maps represent a great advance for regional planning, finer scale maps for cities, as well as improvements in knowledge and communication on climate projections for municipal and land-use decision processes, are still needed. Using the city of Portoviejo and its river watercatchment, we aim to develop a method for augmenting the resolution scale of dynamic CC projections and maps by MAAE, from a resolution of 10 km (10 × 10 km) to 30 m (30 × 30 m) using digital elevation models and Landsat 4/5/7/8 satellite imagery.

Structured in four sections, our paper first describes (in section 2) the data used for reducing the resolution scale of dynamic scale reduction projections by MAAE, detailing each of the steps for detecting satellite images' outliers as well as the procedure for approximating surface to air temperature and extrapolation methods of air temperature time series in time ranges from 1981 to 2040. The methods of adjusting the resulting satellite images with the dynamic scale reduction projections by MAAE are validated using local meteorological stations in Portoviejo. Section 3 presents the resulting maps at a resolution of 30 m and section 4 discusses the method

in the light of the literature review on CC downscaling scales below 5 km, highlighting a series of recommendations for further application and future research.

2. Methods and data

2.1. Data

This work is focused on the city of Portoviejo and its watershed. This is framed by the referential geographical coordinates of: 1°03′16″ S and 80°27′16″ W. Table 2 describes the coordinates of Portoviejo's river watershed and the polygon set for the further steps.

The point of departure for the development of this method is defined by: (a) MAAE's CC dynamic scale reductions of air temperature (mean, maximum and minimum) for RCP 4.5 and RCP 8.5 at 10 × 10 km for the period 2011–2040; (b) air temperatures recorded at the meteorological station of Portoviejo city between 1981 and 2010; and (c) the climate history of air temperature for the period 1981–2005 [36]. The reference position of the meteorological station used has the following coordinates: latitude: 1°02′26″ and longitude: 80°27′54″ [37].

In order to augment the pixel resolution of MAAE's projections, satellite images were obtained from the Climate Engine Platform (http://climateengine.org/) filtering those from Landsat 4/5/7/8 Top of Atmosphere [38]. Landsat's available images included the time range of 1997–2019, with a pixel resolution of 30 m. Finally, altitude was calculated with the digital elevation model STRM [39, 40].

2.2. Outlier detection in satellite images

The outlier detection consisted of identifying the physical limits of the annual and monthly air temperatures [41–43]. In this work, the admissible range for air temperature was defined by the climatological behaviour of the meteorological station in Portoviejo, where the mean, maximum and minimum values are showed in table 3.

Table 3. Central tendency of meteorological station from Portoviejo (referential code station M0005).

	TMIN	TMED	TMAX
Mean	21.6	25.4	31.3
Median	21.5	25.5	31.3
Mode	21.6	24.6	31.7
Maximum	24.5	27.9	33.8
Minimum	19.1	22.9	28.1

It is important to note that, according to the definition of the World Meteorological Organization, 'air temperature' is registered at a height of 2 m above the surface [44].

In satellite images, values detected as 'no data' were considered as outliers, others were detected by the minimum and maximum values estimated from temporal series of air temperature recorded at the Portoviejo station within the period 1981–2010. The range of possible temperatures considered in this work was calculated between 18 °C and 38 °C.

Land Surface Temperature (LST) obtained by satellite images reported a considerable number of outliers (see figure 1) for the year 1997, with decreasing numbers up to 2015.

In order to overcome the missing data from outliers in previous years, we developed an automatized algorithm that recognized LST outliers of all satellite images by using equation (1):

$$\text{outlier} = \begin{cases} {}^{i,j}T_s < 18°C \\ 38°C < {}^{i,j}T_s \end{cases} \Rightarrow {}^{i,j}T_s = -999 \quad (1)$$

where, i and j are the pixel values of each row and column of minimum, maximum and mean LST, respectively. The pixel resolution of Landsat images was 30 m, which according to the study's extension frame shown in table 2, totalled 8696 490 pixel values. Considering that satellite imagery is prone to a number of error data due, for example, to the presence of clouds, outliers were completed (filled-in) with the neighbourhood method as described by Chen *et al* [45] and as depicted in figure 2.

The corresponding neighbourhood analysis equation for filling-in, exemplified in figure 2, is specified in equation (2):

$$\text{Filler} = \sum_{k=1}^{NR} \frac{{}^{i-\frac{NR-1}{2}+k,\,j-\frac{NR-1}{2}+k}T_s}{NR - H}$$
$$\Leftrightarrow {}^{i-\frac{NR-1}{2}+k,\,j-\frac{NR-1}{2}+k}T_s > 0 \quad (2)$$

where, H is the outlier data in $[1, NR]$, $(NR-1)/2$ is the approximated integer number to count the values of temperature registered by the satellite image, as a neighbourhood analysis to calculate each cell of the given raster image. The outlier is filled-in with
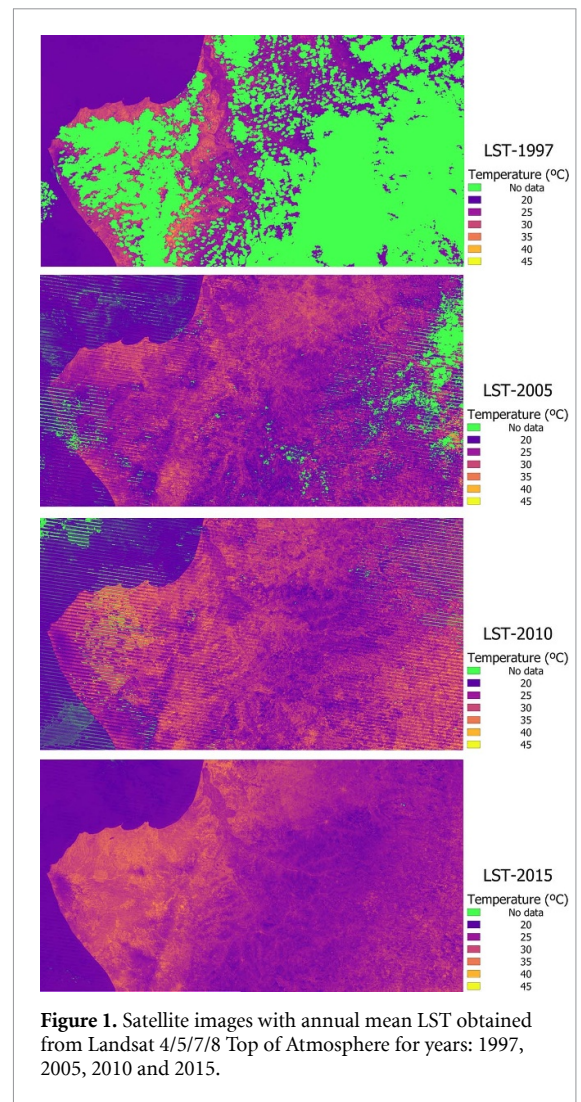
Figure 1. Satellite images with annual mean LST obtained from Landsat 4/5/7/8 Top of Atmosphere for years: 1997, 2005, 2010 and 2015.
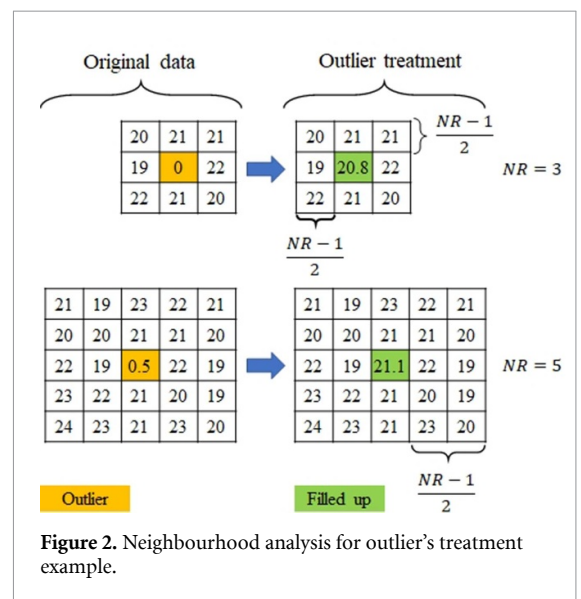
Figure 2. Neighbourhood analysis for outlier's treatment example.

equation (2), however, the outlier data H may be equal to the NR value. The algorithm is iterative and ends when the number of outliers reaches zero (see figure 3).

Figure 3. Flux diagram for the outlier treatment of LST from Landsat 4/5/7/8 satellite images.
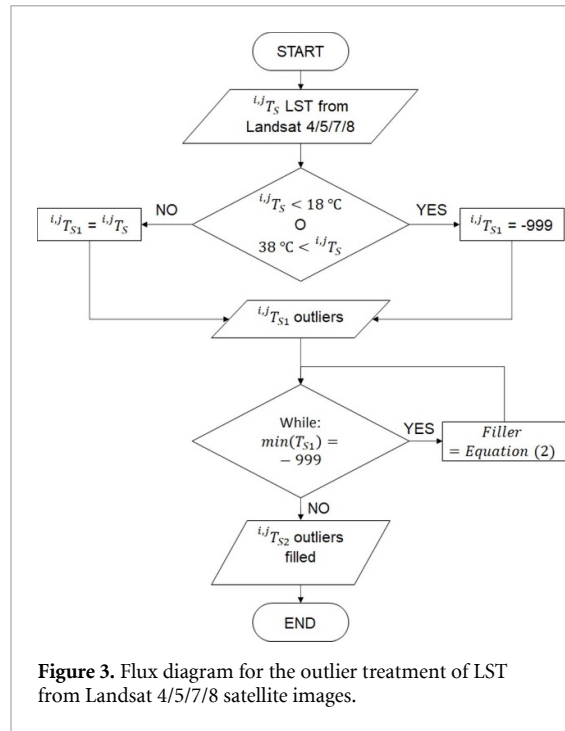
Figure 2 shows how outlier data are detected and filled-in with equation (2), being $^{i,j}T_{s2}$ the outcome raster by this process. This procedure is applied to every single LST satellite image as obtained from Landsat 4/5/7/8 in the yearly range 1997–2019.

2.3. Air temperature approximation at 2 m height from surface level

Air temperature was approximated from the LST and based on Stefan Boltzmann's law, which essentially defines the Earth as a thermal emitter. With this assumption, the maximum irradiance emitted as superficial temperature was set and defined by equation (3) [46, 47]:

$$R_S = \varepsilon_0 \sigma T_S^4 \qquad (3)$$

where, R_S is the emitted radiation by the surface or LST T_S, ε_0 is the emissivity coefficient of the surface and σ is Stefan Boltzmann's constant. Alves *et al* [47], estimate the surface emissivity as described under equation (4):

$$\varepsilon_0 = 0.95 + 0.01\,(\text{LAI}) \qquad (4)$$

where, LAI is the leaf area index based on data from Landsat satellite images, as it was suggested by Alves *et al* [47]. The air temperature system is modelled as a surface that emits radiation according to Stefan Boltzmann's law and is expressed as shown by equation (5):

$$R_a = \varepsilon_a \sigma T_a^4 \qquad (5)$$

where, R_a is the emitted radiation by the air, ε_a is the air emissivity and T_a is the air temperature. In this work, R_a is approximated by the Beer Lambert

law $(R_a = R_s \exp(\delta))$, where δ is the optical depth estimated by the atmosphere transmittance according to $\ln(1/\tau_{SW})$ [48]. The emissivity coefficient of air is expressed in equation (6):

$$\varepsilon_a = 0.85[-\ln(\tau_{SW})]^{0.09}. \qquad (6)$$

In equation (6), τ_{SW} is the atmosphere transmittance for clear sky. Resulting values work only with satellite images that have no LST outliers and have been filled-in as described in figure 2. In the work of Waters *et al* [46], transmittance is approximated by the mathematical relation expressed in equation (7):

$$\tau_{SW} = 0.75 + 2\,(H+2)\,10^{-5} \qquad (7)$$

where, $(H+2)$ corresponds to the digital elevation model STRM (DEM) at 2 m from the land surface, with a pixel resolution of 30 m. Air temperature is thus estimated and followed by applying equations (5) and (6), where the input data are the raster of LST, the vegetation index and the digital elevation model.

2.4. Extrapolation of air temperature time series in the years 1981–2040

There are several ways to extrapolate time series according to statistical behaviour; however, the most common is based on trends and is a linear interpolation with least squares [49, 50]. Other, non-linear methods are more complex (see Mudelsee [49]) where the use of regression analysis under quadratic, polynomial, sinusoidal, and power, among other equations, challenges the ability to recognize such trends. This type of model allows to predict values in the near future or fill-in outliers in datasets. However, an important limitation of this type of analysis is extrapolating the time series to the far future, where mathematical functions may diverge, and uncertainty becomes an increasing concern.

For the purpose of this research, extrapolation of air temperature in time was estimated with the use of Fourier's series. Equation (8) was used for the calculation and analysis of Fourier series' as follows:

$$f(x) = \frac{a_0}{2} + \sum_{i=1}^{\infty} a_i \cos\left(\frac{2i\pi x}{T}\right) + b_i \text{sen}\left(\frac{2i\pi x}{T}\right) \qquad (8)$$

where, T is the period, i are the amornics, x is the temporal series to be analysed, a_i and b_i are the Fourier coefficients. A higher number of i implies a better fit of the Fourier series over the air temperature temporal series [51, 52]. In the present work, a_i and b_i coefficients are approximated with least squares and the period is equivalent to the range of years analysed

and available from Landsat images. In this context, equation (8) was reformulated as shown in equation (9):

$$y_j = \sum_{i=1}^{\infty} a_{(2i-1)} f_{(2i-1)}\left(x_j\right) + a_{(2i)} f_{(2i)}\left(x_j\right). \quad (9)$$

In equation (9), y_j are the values of air temperature, x_j are the range of years (1981–2040) considered in the analysis, $a_{(2i-1)}$ y $a_{(2i)}$ are the coefficients to be determined with least squares. The functions related

to Fourier's series in equation (9) are expressed in equation (10):

$$f_{(2i-1)}\left(x_j\right) = \cos\left(\frac{2i\pi x_j}{T}\right)$$

$$f_{(2i)}\left(x_j\right) = \text{sen}\left(\frac{2i\pi x_j}{T}\right). \quad (10)$$

Following from equation (10), the least squares method, determining the interpolation coefficients was solved by the resolution of the matrix shown in equation (11):

$$
\begin{bmatrix}
f_1(x_1) & f_2(x_1) & f_3(x_1) & \cdots & f_{(2i-1)}(x_1) & f_{(2i)}(x_1) \\
f_1(x_2) & f_2(x_2) & f_3(x_2) & \cdots & f_{(2i-1)}(x_2) & f_{(2i)}(x_2) \\
f_1(x_2) & f_2(x_2) & f_3(x_3) & \cdots & f_{(2i-1)}(x_3) & f_{(2i)}(x_3) \\
\vdots & \vdots & \vdots & \ddots & \vdots & \vdots \\
f_1(x_{j-1}) & f_2(x_{j-1}) & f_3(x_{j-1}) & \cdots & f_{(2i-1)}(x_{j-1}) & f_{(2i)}(x_{j-1}) \\
f_1(x_j) & f_2(x_j) & f_3(x_j) & \cdots & f_{(2i-1)}(x_j) & f_{(2i)}(x_j)
\end{bmatrix}
\cdot
\begin{Bmatrix}
a_1 \\ a_2 \\ a_3 \\ \vdots \\ a_{(2i-1)} \\ a_{(2i)}
\end{Bmatrix}
=
\begin{Bmatrix}
y_1 \\ y_2 \\ y_3 \\ \vdots \\ y_{j-1} \\ y_j
\end{Bmatrix}. \quad (11)
$$

Equation (11) can be solved if $j \geqslant 2i$, assuring that N equations with N unknowns can be solved following the well-known procedure of Gauss Jordan.

2.5. Pixels adjusted between satellite images projected in time vs climate change projections of MAAE

Adjusting pixels consisted of comparing air temperature maps (30 m) obtained from Landsat and those from MAAE (10 km) (RCP 4.5 and RCP 8.5 [53, 54]). Figure 4 shows the 10 km pixel resolution of air temperature for January 2000 as published by MAAE.

Adjusting the pixels from Landsat air temperature images with those projected for RCP 4.5 and 8.5 entailed rescaling the 30 m pixel resolution found on every pixel with those pixels' resolution of 10 km, following the expression of equation (12):

$$b_{ij} = \frac{a_{ij}}{\bar{a}}\bar{X}$$

$$\bar{b} = \frac{1}{NM}\sum_{i=1}^{N}\sum_{j=1}^{M} b_{ij} = \bar{X}. \quad (12)$$

In equation (12), $\bar{X}$ is the air temperature value of maps with pixel resolution of 10 km, a_{ij} are the pixels with resolution of 30 m found in $\bar{X}$, b_{ij} are the pixels rescaled, $\bar{a}$ is the mean of the a_{ij} values, N and M are the maximum number of rows and columns for i and j, respectively.

2.6. Validation of the high-resolution model of climate projection

The validation of the resulting map with the high-resolution model for CC projections at a 30 m

resolution consisted of comparing the temporal series of air temperatures obtained with the data registered by the meteorological station in Portoviejo [37]. Figure 5 shows the flux diagram for the validation process.

In figure 5, $^{k}T_a$ and $^{k}T_a{}'$ are the air temperature values obtained from the meteorological station in Portoviejo and the final map obtained from the high-resolution model, respectively. The interval specified in figure 5 covers 95% of the temporal series of each pixel within a normal distribution. This procedure guaranteed that the high-resolution model satisfies the Student's t-test with data from the meteorological station in the period 1981–2005 for mean air temperature.
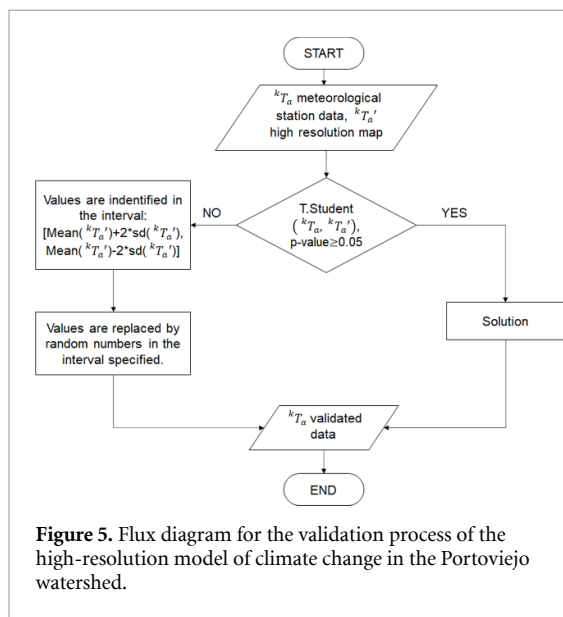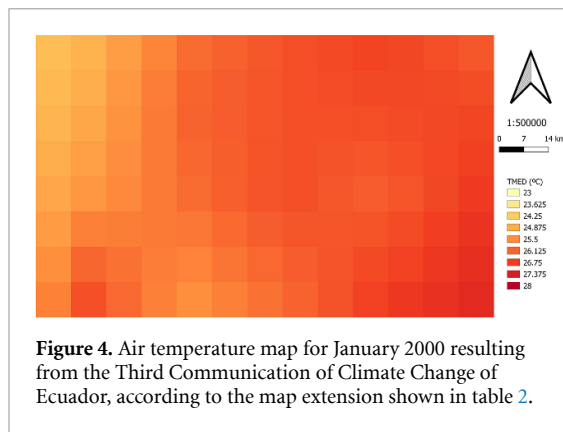
3. Results

Following the procedure described in figure 3, resulting LST maps between 1997 and 2019 are shown in figure 6.

LST maps in figure 6, ranging from 1997 to 2015, show that at least for 1997, outliers reduced the quality and image resolution of this map. This behaviour can also be observed when using maximum and minimum LSTs. In the case of 2010 onwards, the number of outliers falls considerably, thus increasing the reliability of the resulting maps.

As for air temperature, this is estimated from LST according to equations (5) and (6) resulting in maps as shown in figure 7.

Figure 7 shows the mean air temperature approximated with Stefan Boltzmann's law, extrapolated in time as a function of Fourier's series and following

Figure 4. Air temperature map for January 2000 resulting from the Third Communication of Climate Change of Ecuador, according to the map extension shown in table 2.

Figure 5. Flux diagram for the validation process of the high-resolution model of climate change in the Portoviejo watershed.

Figure 6. Maps of mean land surface temperature for years 1997, 2005, 2010 and 2015.

Figure 7. Mean of air temperature in the period 1981–2005, estimated from LST with equations (5) and (6) with a pixel resolution of 30 m.

the procedure of pixel adjustment between satellite images (30 m) and CC projections (10 km). According to the meteorological station in Portoviejo city, air temperature data were validated following the procedure illustrated in figure 5.
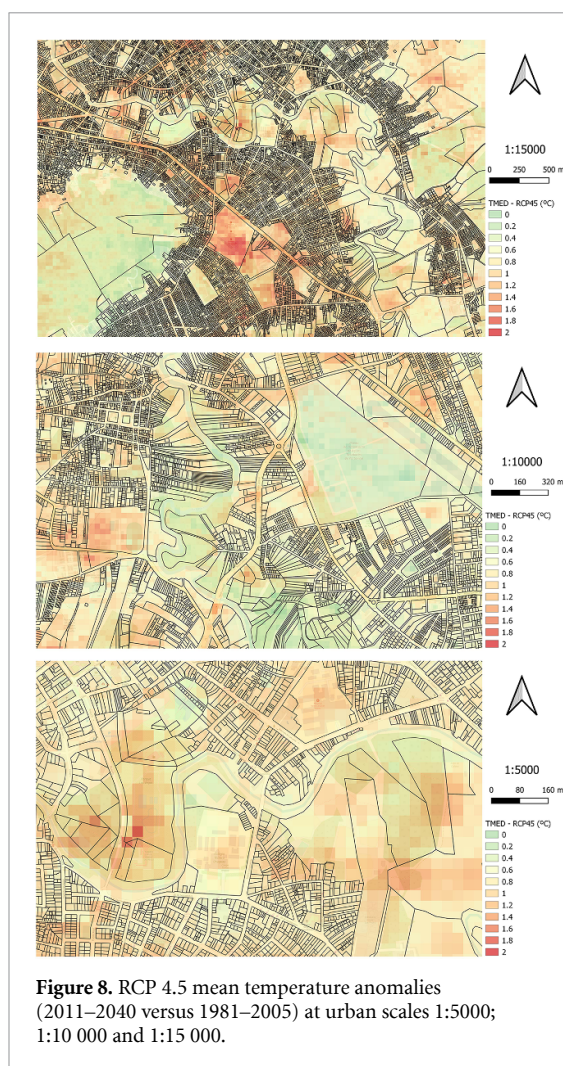
Student's *t*-test was applied to (a) meteorological station data for mean air temperature in the period 1981–2005 vs MAAE's model (WRF DDS) and (b) meteorological station data for mean air temperature in the period 1981–2005 vs the high-resolution model. *P*-value results within (a) are close to zero, below 0.05, suggesting observational unlikelihood, and for (b) report values near to 0.095, demonstrating observational likelihood. The mean air temperature of meteorological station is 25.4 (°C), (a) 25.9 (°C), and (b) 25.6 (°C).

Figure 8 shows the anomalies (RCP 4.5 2011–2040 vs 1981–2005) for mean air temperature at random places in Portoviejo city, with scales 1:15 000, 1:10 000 and 1:5000. It is possible to observe that the highest values of anomalies correspond to the places with a high percentage of buildings; the river, parks and green infrastructure registered the lowest. These maps provide high-quality information for land-use and urban planning in Portoviejo city.
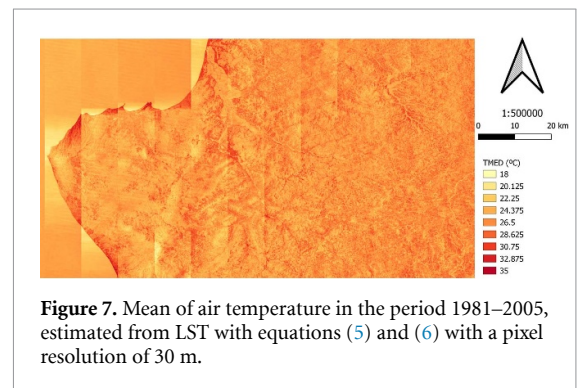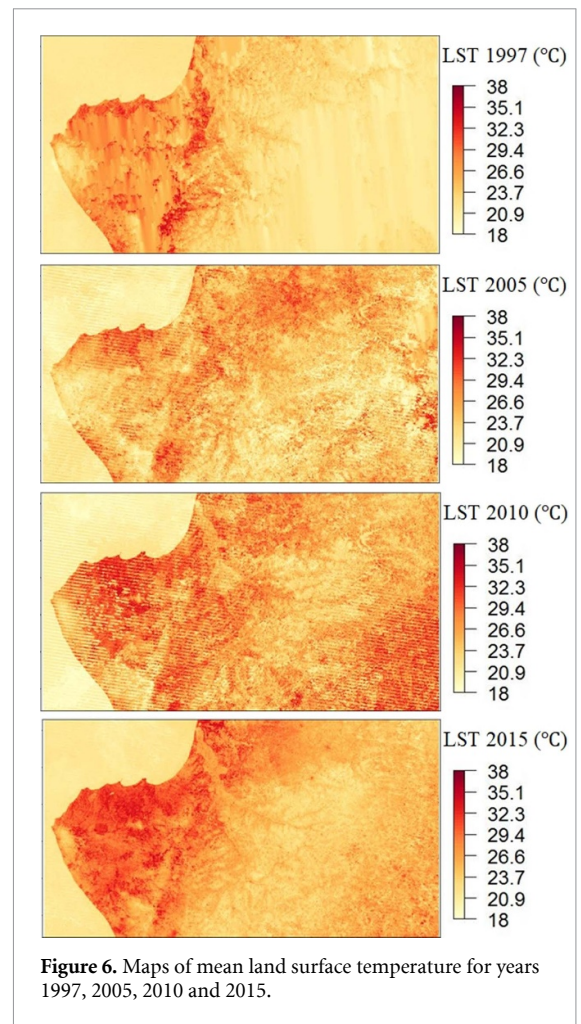
4. Discussion and conclusions

Having defined the spatial boundaries at watershed scale, our model complements those perspectives in addressing the ecological environment, water quality, and ecological flows [34] as well as territorial dynamics. The final CC maps have an augmented resolution, showing coherence with those of MAAE, and offering a low-cost method for demonstrating temperature anomalies due to CC to land-use and urban planners, as well as local development decision makers. This information can be used for both mitigation and adaptation measures implemented by municipal

Figure 8. RCP 4.5 mean temperature anomalies (2011–2040 versus 1981–2005) at urban scales 1:5000; 1:10 000 and 1:15 000.

Table 4. Constraints and challenges in reducing scales among climatic projections.

Constraints/challenges	Authors
Model requires validation before using	Hu and Ayyub [55]
Difficulties of validating model under dynamic scenario	Bormann [56]; Kusaka *et al* [30]; Hamdi *et al* [29]; Lemonsu *et al* [32]; Oliveira *et al* [13]; Shastri *et al* [19]
Uncertainties regarding data dynamics	Chandra *et al* [57]
Difficulties of replicating data	Gulacha and Mulungu [58]
Difficulties of collecting a large number of variables	Gu *et al* [7]; Su *et al* [20]
Data interpolation undermines the model quality	Didovets *et al* [5]
Uncertainty regarding model selection and results	Khalyani *et al* [9]; Su *et al* [21]; Aich *et al* [3]
RPC 4.5 scenario hinders insights into future temperatures	Rana and Moradjkani (2015); Bastin *et al* [27]
Difficulties of predicting future scenarios	Yan *et al* [34]
Topography is a challenge to the use of Regional Concentration Models (RCMs)	Prömmel *et al* [14]; Sanjay *et al* [17]
RCM outputs present bias	Worku *et al* [59]
WRF and statistical downscaling methods need improvements	Jahangir and Moghim [8]; Tang *et al* [22]
Uncertainties regarding model downscaling procedures	Varikoden *et al* [23]
Difficulties of combining downscaling models	Mathis *et al* [11]; Akhter *et al* [4]
Limitations of hardware and software capabilities make full-scale modelling for a city difficult	Ramyar *et al* [15]
Scale heterogeneity hinders the quality of the study	McCarthy *et al* [12]; Reshmidevi *et al* [33]
Scientific findings are difficult for society to understand	Kjellström *et al* [10]
Combination of models enables consistency of the procedures and methods	Hu and Ayyub [55]; Hasan *et al* [28]; Seiler *et al* [18]

governments as part of their development projects. This would be useful for inland analysis, whereas coastal areas are not necessarily recognized by the CC projections of WRF (MAAE). Observing an increasing trend in the scope of CC financing to cities, the method developed here offers a clear baseline for CC financing and investment to be tailored to local needs and scales. The series of constraints and challenges in reducing scales among climate projections (see table 4), and particularly those mentioned by Oliveira *et al*, Shastri *et al*, Hamdi *et al*, Kusaka *et al*, Lemonsu *et al*, Bormann [13, 19, 29, 30, 32, 56] on validating dynamic scenarios, were observed. In terms of our results, the model offers further research possibilities, for example in adding variables that consider urban sprawl, mobility patterns, urban densities, etc, which would increase accuracy. Nonetheless, when considering the technical limitations of hardware and software capabilities for most municipalities, as described by Ramyar *et al* [15], as well as the urgency of localizing CC at the urban scale, the resulting maps can go down to at least 1:1000 in scale (see, e.g. figure 8). As a scientifically sound means of communication, these maps contribute to incorporating CC data into planning

as well as into development narratives at municipal scale. Based on existing CC projections at national/regional scale, the method and maps developed here are based on open access satellite imagery which can easily be made available to land-use planning decision makers at a resolution of 30 × 30 m, consistent with the dynamic downscaling maps for RCP 4.5 and 8.5 by MAAE at different scales (see, e.g. figure 9). Beyond their possible impact on policy making and CC mitigation and adaption measures at the local scale, such maps can also be employed on new land-use configurations, including nature-based
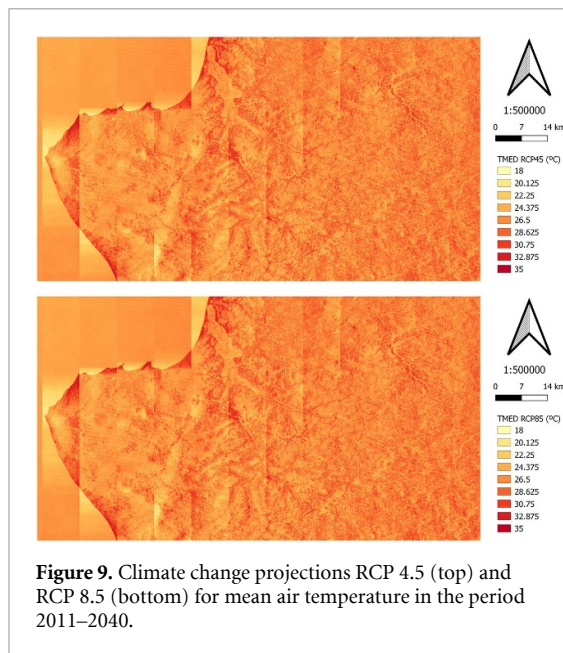
Figure 9. Climate change projections RCP 4.5 (top) and RCP 8.5 (bottom) for mean air temperature in the period 2011–2040.

solutions, energy demand scenarios, energy efficiency measures, etc.

Data availability statement

The data that support the findings of this study are available upon reasonable request from the authors.

ORCID iDs

Juan Diego Jijón ⬛ https://orcid.org/0000-0001-7013-423X

Karl-Heinz Gaudry ⬛ https://orcid.org/0000-0001-7925-5150

Jessica Constante ⬛ https://orcid.org/0000-0003-2123-8432

References

[1] Smid M and Costa A C 2018 Climate projections and downscaling techniques: a discussion for impact studies in urban systems *Int. J. Urban Sci.* **22** 277–307

[2] Adham A, Wesseling J G, Abed R, Riksen M, Ouessar M and Ritsema C J 2019 Assessing the impact of climate change on rainwater harvesting in the Oum Zessar watershed in Southeastern Tunisia *Agric. Water Manage.* **221** 131–40

[3] Aich V, Liersch S, Vetter T, Fournet S, Andersson J C M, Calmanti S, van Weert F H A, Hattermann F F and Paton E N 2016 Flood projections within the Niger River Basin under future land use and climate change *Sci. Total Environ.* **562** 666–77

[4] Akhter M S, Shamseldin A Y and Melville B W 2019 Comparison of dynamical and statistical rainfall downscaling of CMIP5 ensembles at a small urban catchment scale *Stoch. Environ. Res. Risk Assess.* **33** 989–1012

[5] Didovets I, Krysanova V, Bürger G, Snizhko S, Balabukh V and Bronstert A 2019 Climate change impact on regional floods in the Carpathian region *J. Hydrol. Reg. Stud.* **22** 100590

[6] Fitzpatrick M C and Dunn R R 2019 Contemporary climatic analogs for 540 North American urban areas in the late 21st century *Nat. Commun.* **10** 1–7

[7] Gu L, Chen J, Xu C-Y, Kim J-S, Chen H, Xia J and Zhang L 2019 The contribution of internal climate variability to climate change impacts on droughts *Sci. Total Environ.* **684** 229–46

[8] Jahangir M S and Moghim S 2019 Assessment of the urban heat island in the city of Tehran using reliability methods *Atmos. Res.* **225** 144–56

[9] Khalyani A H, Gould W A, Harmsen E, Terando A, Quinones M and Collazo J A 2016 Climate change implications for tropical islands: interpolating and interpreting statistically downscaled GCM projections for management and planning *J. Appl. Meteorol. Climatol.* **55** 265–82

[10] Kjellström E, Bärring L, Nikulin G, Nilsson C, Persson G and Strandberg G 2016 Production and use of regional climate model projections—a Swedish perspective on building climate services *Clim. Serv.* **2–3** 15–29

[11] Mathis M, Elizalde A and Mikolajewicz U 2018 Which complexity of regional climate system models is essential for downscaling anthropogenic climate change in the Northwest European Shelf? *Clim. Dyn.* **50** 2637–59

[12] McCarthy M P, Harpham C, Goodess C M and Jones P D 2012 Simulating climate change in UK cities using a regional climate model, HadRM3 *Int. J. Climatol.* **32** 1875–88

[13] Oliveira G G, Pedrollo O C and Castro N M R 2015 Stochastic approach to analyzing the uncertainties and possible changes in the availability of water in the future based on scenarios of climate change *Hydrol. Earth Syst. Sci.* **19** 3585–604

[14] Prömmel K, Cubasch U and Kaspar F 2013 A regional climate model study of the impact of tectonic and orbital forcing on African precipitation and vegetation *Palaeogeogr. Palaeoclimatol. Palaeoecol.* **369** 154–62

[15] Ramyar R, Zarghami E and Bryant M 2019 Spatio-temporal planning of urban neighborhoods in the context of global climate change: lessons for urban form design in Tehran, Iran *Sustain. Cities Soc.* **51** 101554

[16] Rodriguez-Lloveras X, Buytaert W and Benito G 2016 Land use can offset climate change induced increases in erosion in Mediterranean watersheds *CATENA* **143** 244–55

[17] Sanjay J, Krishnan R, Shrestha A B, Rajbhandari R and Ren G-Y 2017 Downscaled climate change projections for the Hindu Kush Himalayan region using CORDEX South Asia regional climate models *Adv. Clim. Change Res.* **8** 185–98

[18] Seiler C, Zwiers F W, Hodges K I and Scinocca J F 2018 How does dynamical downscaling affect model biases and future projections of explosive extratropical cyclones along North America's Atlantic coast? *Clim. Dyn.* **50** 677–92

[19] Shastri H, Ghosh S, Paul S, Shafizadeh-Moghadam H, Helbich M and Karmakar S 2019 Future urban rainfall projections considering the impacts of climate change and urbanization with statistical–dynamical integrated approach *Clim. Dyn.* **52** 6033–51

[20] Su B, Huang J, Gemmer M, Jian D, Tao H, Jiang T and Zhao C 2016 Statistical downscaling of CMIP5 multi-model ensemble for projected changes of climate in the Indus River Basin *Atmos. Res.* **178–179** 138–49

[21] Su B, Jian D, Li X, Wang Y, Wang A, Wen S, Tao H and Hartmann H 2017 Projection of actual evapotranspiration using the COSMO-CLM regional climate model under global warming scenarios of 1.5°C and 2.0°C in the Tarim River basin, China *Atmos. Res.* **196** 119–28

[22] Tang J, Niu X, Wang S, Gao H, Wang X and Wu J 2016 Statistical downscaling and dynamical downscaling of regional climate in China: present climate evaluations and future climate projections *J. Geophys. Res.* **121** 2110–29

[23] Varikoden H, Mujumdar M, Revadekar J V, Sooraj K P, Ramarao M V S, Sanjay J and Krishnan R 2018 Assessment of regional downscaling simulations for long term mean, excess and deficit Indian Summer Monsoons *Glob. Planet. Change* **162** 28–38

[24] Wang X, Huang G, Lin Q, Nie X, Cheng G, Fan Y, Li Z, Yao Y and Suo M 2013 A stepwise cluster analysis approach for downscaled climate projection—a Canadian case study *Environ. Model. Softw.* **49** 141–51

[25] Zhou X, Huang G, Wang X, Fan Y and Cheng G 2018 A coupled dynamical-copula downscaling approach for temperature projections over the Canadian Prairies *Clim. Dyn.* **51** 2413–31

[26] Argüeso D, Evans J P, Fita L and Bormann K J 2014 Temperature response to future urbanization and climate change *Clim. Dyn.* **42** 2183–99

[27] Bastin J-F *et al* 2019 Understanding climate change from a global analysis of city analogues *PLoS One* **14** e0217592

[28] Hasan A, Binti Pg D, Ratnayake U, Shams S, Nayan Z B H and Rahman E K A 2018 Prediction of climate change in Brunei Darussalam using statistical downscaling model *Theor. Appl. Climatol.* **133** 343–60

[29] Hamdi R, Hv D V, Rd T and Termonia P 2014 Assessment of three dynamical urban climate downscaling methods: brussels's future urban heat island under an A1B emission scenario *Int. J. Climatol.* **34** 978–99

[30] Kusaka H, Hara M and Takane Y 2012 Urban climate projection by the WRF model at 3-km horizontal grid increment: dynamical downscaling and predicting heat stress in the 2070's august for tokyo, osaka, and nagoya metropolises *J. Meteorolog. Soc. Japan* II **90B** 47–63

[31] Lauwaet D, Hooyberghs H, Maiheu B, Lefebvre W, Driesen G, Van Looy S and De Ridder K 2015 Detailed urban heat island projections for cities worldwide: dynamical downscaling CMIP5 global climate models *Climate* **3** 391–415

[32] Lemonsu A, Kounkou-Arnaud R, Desplat J, Salagnac J-L and Masson V 2012 Evolution of the Parisian urban climate under a global changing climate *Climatic Change* **116** 679–92

[33] Reshmidevi T V, Nagesh Kumar D, Mehrotra R and Sharma A 2018 Estimation of the climate change impact on a catchment water balance using an ensemble of GCMs *J. Hydrol.* **556** 1192–204

[34] Yan T, Bai J, Arsenio T, Liu J and Shen Z 2019 Future climate change impacts on streamflow and nitrogen exports based on CMIP5 projection in the Miyun reservoir basin, China *Ecohydrol. Hydrobiol.* **19** 266–78

[35] Skamarock W, Klemp J, Dudhia J, Gill D, Barker D, Wang W, Huang X-Y and Duda M 2008 A Description of the Advanced Research WRF Version 3 UCAR/NCAR (http://dx.doi.org/10.5065/D68S4MVH)

[36] Ministerio del Ambiente de Ecuador, Instituto Nacional de Meteorología e Hidrología y Universidad de Cuenca 2016 Generación de proyecciones climáticas para la 'Tercera Comunicación Nacional de Cambio Climático de Ecuador' (Quito-Ecuador: bajo los escenarios de emisión RCP del reporte AR5 del IPCC)

[37] Instituto Nacional de Meteorología e Hidrología del Ecuador INAMHI (available at: www.servicio meteorologico.gob.ec/) (Accessed 5 April 2020)

[38] Huntington J L *et al* 2017 Climate engine: cloud computing and visualization of climate and remote sensing data for advanced Natural resource monitoring and process understanding *Bull. Am. Meteorol. Soc.* **98** 2397–410

[39] International Centre for Tropical Agriculture (CIAT) 2008 Hole-filled seamless SRTM data V4 Hole-filled seamless SRTM data V4 Jarvis A, Reuter H I, Nelson A and Guevara E SRTM Data—CGIAR-CSI SRTM (available at: https://srtm.csi.cgiar.org) (Accessed 16 September 2019)

[40] Farr Tom G 2007 The Shuttle Radar Topography Mission *Rev. Geophys.* **45** 1–33

[41] Stepanek P, Zahradnıcek P and Skalak P 2009 Data quality control and homogenization of air temperature and precipitation series in the area of the Czech Republic in the period 1961–2007 *Adv. Sci. Res.* **3** 23–26

[42] Venema V K C *et al* 2013 Benchmarking homogenization algorithms for monthly data *AIP Conf. Proc.* **1552** 1060–5

[43] Vejen F, Jacobsson C, Fredriksson U, Moe M, Andresen L, Hellsten E, Rissanen P, Palsdóttir T and Arason T 2002 Quality Control of meteorological observations—automatic methods used in the nordic countries. Oslo

[44] World Meteorological Organization WMO 2018 *Guide to Meteorological Instruments and Methods of Observation* (https://library.wmo.int/doc_num.php?explnum_id\protect$\relax=$10616) (Access 20 May 2020)

[45] Chen J *et al* 2014 Global land cover mapping at 30 m resolution: a POK-based operational approach *ISPRS J. Photogramm. Remote Sens.* **103** 7–27

[46] Waters R, Allen R, Bastiaanssen W, Tasumi M and Trezza R 2002 *S E B A L Sebal (Surface Energy Balance Algorithms for Land)—Advanced Training and Users Manual—Idaho Implementation*

[47] Alves L E R de Freita IGF, Gomes HB, Dos S Silva FD, Dos Santos MN 2017 Using Landsat-8 images in the estimation of the surface radiation balance *J. Hyperspectral Remote Sens.* **7** 91–100

[48] Horvath H 2016 Light absorption in the atmosphere *Light Scattering Reviews 10: Light Scattering and Radiative Transfer* ed A A Kokhanovsky (Berlin: Springer) pp 235–89

[49] Mudelsee M 2019 Trend analysis of climate time series: a review of methods *Earth-Sci. Rev.* **190** 310–22

[50] Reeves J, Chen J, Wang X L, Lund R and Lu Q Q 2007 A review and comparison of changepoint detection techniques for climate data *J. Appl. Meteorol. Climatol.* **46** 900–15

[51] Livezey R E, Vinnikov K Y, Timofeyeva M M, Tinker R, Van Den Dool H M, Livezey R E, Vinnikov K Y, Timofeyeva M M Tinker R and van den Dool HM 2007 Estimation and extrapolation of climate normals and climatic trends *J. Appl. Meteorol. Climatol.* **46** 1759–76

[52] Jakubauskas M E and Legates D R 2000 Harmonic analysis of time-series AVHRR NDVI data for characterizing US great plains land use/land cover *Int. Arch. Photogramm. Remote Sens.* **33** 384–9

[53] Pachauri R K and Meyer L A Intergovernmental Panel on Climate Change (IPCC) 2014 Fifth Assessment Report (available at: www.ipcc.ch/assessment-report/ar5/) (Accessed 9 October 2019)

[54] Ministerio del Ambiente y Agua 2017 Tercera Comunicación Nacional del Ecuador Tercera Comunicación Nacional del Ecuador (available at: www.ambiente.gob.ec/tercera-comunicacion-nacional-del-ecuador/) (Accessed 16 September 2019)

[55] Hu H and Ayyub B M 2019 Machine Learning for Projecting Extreme Precipitation Intensity for Short Durations in a Changing Climate *Geosciences* **9** 209

[56] Bormann H 2012 Assessing the soil texture-specific sensitivity of simulated soil moisture to projected climate change by SVAT modelling *Geoderma* **185–186** 73–83

[57] Chandra R, Saha U and Mujumdar P 2015 Model and parameter uncertainty in IDF relationships under climate change *Adv. Water Res.* **79** 127–39

[58] Gulacha M M and Mulungu D M M 2017 Generation of climate change scenarios for precipitation and temperature at local scales using SDSM in Wami-Ruvu River Basin Tanzania *Physics and Chemistry of the Earth, Parts A/B/C* **100** 62–72

[59] Worku G, Teferi E, Bantider A, Dile Y T and Taye M T 2018 Evaluation of regional climate models performance in simulating rainfall climatology of Jemma sub-basin, Upper Blue Nile Basin, Ethiopia *Dynamics of Atmospheres and Oceans* **83** 53–63